JOURNAL OF MATERIALS SCIENCE **35** (2000) 3599–3606

A new route to synthesize $La_{1-x}Sr_xMnO_3$

Q. MING, M. D. NERSESYAN, J. T. RICHARDSON, DAN LUSS*
Department of Chemical Engineering, University of Houston, Houston TX 77204-4792, USA
E-mail: dluss@uh.edu

A. A. SHIRYAEV
Institute of Structural Microkinetics, Russian Academy of Sciences, Chernogolovka, 142432, Russia

Self-Propagating High-temperature Synthesis (SHS) was used to produce complex oxides ($La_{1-x}Sr_xMnO_3$ with $x = 0$, 0.1 and 0.2), which are used as the cathode in solid oxide fuel cells (SOFCs). Thermodynamic predictions and experiments show that $La_{1-x}Sr_xMnO_3$ can be prepared via SHS under moderate conditions from a mixture of $La_2O_3 + SrO_2 + Mn$, using either gaseous oxygen or solid $NaClO_4$ as the oxidant. Partial melting at the high combustion temperature increased product homogeneity. The electrical conductivity of the product was 180 $S \cdot cm^{-1}$ at 1000 °C in air, matching that of sample made by other synthesis processes. SHS enables a more economical production of $La_{1-x}Sr_xMnO_3$ than existing commercial processes.

1. Introduction

Modern solid oxide fuel cells (SOFCs) use cathode tubes made of $La_{1-x}Sr_xMnO_3$ (LSM) [1]. About 4.5 kilograms of LSM are used per kilowatt of power, so that a MW-scale unit requires about 4.5 tons of LSM. This powder is commonly produced by the amorphous citrate process (Pechini method) [2], in which metal salts are dissolved in citric acid/ethylene glycol solution followed by evaporation of the solvent. The residue is heated to decompose and remove the organic residue and to obtain the desired oxide. The process has also been modified by changing the citric acid/ethylene glycol ratio [3–6]. Other synthesis processes are freeze-drying [7], spray pyrolysis [8–10], sol-gel [10, 11] and the glycine-nitrate method [12]. In freeze-drying, metals are dissolved in nitric acid and the solution sprayed into liquid nitrogen, and resulting $LaMnO_3$ powder has a very high surface area (14–32 m^2/g). In the spray pyrolysis process, aqueous nitrate droplets are decomposed in a hot reaction chamber. These wet-chemical processes often involve complicated procedures and also lead to the formation of undesired side products. The high price of LSM is an important component of the manufacturing cost of SOFCs and there is a strong incentive for developing an alternative, more economical method for the production of LSM powder.

SHS can produce many inorganic materials at a lower price than other processes [13]. In this method, solid powders are intimately mixed and pressed into pellets, which are ignited by heating of one end. Heat is released, creating a combustion front which propagates through the pellet forming the desired product. This method offers several important advantages, such as high productivity, low external energy consumption and use of simple production facilities. SHS has been successfully used to synthesize complex oxide materials such as ferrites, high temperature superconductors and other oxides [14–18].

We report here a study on the feasible production of $La_{1-x}Sr_xMnO_3$ (with $x = 0$, 0.1 and 0.2) via SHS. This includes a thermodynamic feasibility analysis of the combustion synthesis, an experimental study of the influence of the synthesis conditions, the mechanism and sequence of the reactions, and phase formation in the combustion wave.

2. Thermodynamic feasibility analysis of combustion synthesis

Thermodynamic feasibility analysis (TFA) gives the equilibrium composition and combustion temperature through minimization of the thermodynamic potential, subject to material and energy balances [13, 19, 20]. We use a TFA to analyze the feasibility of SHS of $La_{1-x}Sr_xMnO_3$ ($x = 0$, 0.1 and 0.2) from the following reactant mixtures, using either gaseous O_2 as the oxidant:

$$La_2O_3 + 2Mn \xrightarrow{O_2} 2LaMnO_3 \quad (1)$$

$$La_2O_3 + (2-y)Mn + yMnO_2 \xrightarrow{O_2} 2LaMnO_3 \quad (2)$$

$$(1-x)La_2O_3 + xSrO_2 + (2-y)Mn + yMnO_2 \xrightarrow{O_2} 2La_{1-x}Sr_xMnO_3 \quad (3)$$

* Author to whom all correspondence should be addressed.

or solid $NaClO_4$ as oxidant:

$$La_2O_3 + 2Mn + 0.75NaClO_4 \rightarrow 2LaMnO_3 + 0.75NaCl\uparrow \quad (4)$$

$$La_2O_3 + (2-y)Mn + yMnO_2 + 0.25(3-2y) \times NaClO_4 \rightarrow 2LaMnO_3 + 0.25(3-2y)NaCl\uparrow \quad (5)$$

$$(1-x)La_2O_3 + xSrO_2 + (2-y)Mn + yMnO_2 + 0.25(3+x-2y)NaClO_4 \rightarrow 2La_{1-x}Sr_xMnO_3 + 0.25(3+x-2y)NaCl\uparrow \quad (6)$$

The TFA of reaction (1) (Fig. 1) shows that the equilibrium temperature increases from about 1970 to 2150 °C as the air pressure is increased from 1 to 4 atm. For all pressures exceeding 3 atm, the product is $LaMnO_3$. The increased pressure suppresses the dissociation of lanthanum oxide, which in turn increases the adiabatic combustion temperature. When solid $NaClO_4$ (Fig. 2) is used as the oxidant, the combustion temperature is lower than when gaseous oxygen is used (Fig. 1). The desired $LaMnO_3$ product is liquid when the air pressure exceeds 8 atm.

The amount of gaseous products may be reduced by diluting the reactant fuel Mn with its oxide (MnO_2) since this decreases the combustion temperature. A TFA of reaction mixture (2) shows that increasing the molar amount of MnO_2 (y) decreases the temperature from about 1970 °C with pure Mn to 1730 °C with 0.6 mole MnO_2 dilution (Fig. 3).

The equilibrium temperature (Fig. 2) is insensitive to the pressure between 1 to 4 atm for the reaction mixture described by Equation 4, and is unaffected by dilution (Fig. 3) for y between 0.2 to 0.5 for the reaction mixture described by Equation 2. This essentially constant temperature at increasing oxygen pressures and dilution is caused by a phase transition, which compensates the change in the combustion heat. The almost constant temperature in Fig. 2 for oxygen pressures between 1 to 4 atm is due to the endothermic phase-transition (melting of the final product) which compensates for the increased heat of combustion. The essentially constant equilibrium temperature region in Fig. 3 is due to an exothermic condensation of LaO_2 and crystallization of liquid $LaMnO_3$, which compensates for the decreased heat of combustion with dilution. The calculated combustion temperatures for reaction (3) are shown in Fig. 4. Since the amount of SrO_2 used is rather small, the combustion temperatures and product compositions as a function of dilution are similar to those of the undoped reaction (2). Only liquid product is obtained when the dilution is less than 0.2 mole due to the high temperature.

The calculated combustion temperatures for three products (Table I) show that using $NaClO_4$ as the

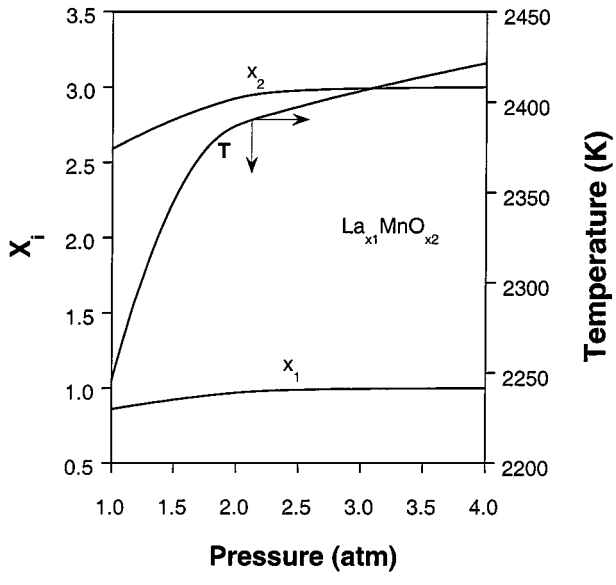

Figure 1 Dependence of the equilibrium temperature and composition of the products formed by the reaction mixture of $La_2O_3 + 2Mn + O_2$.

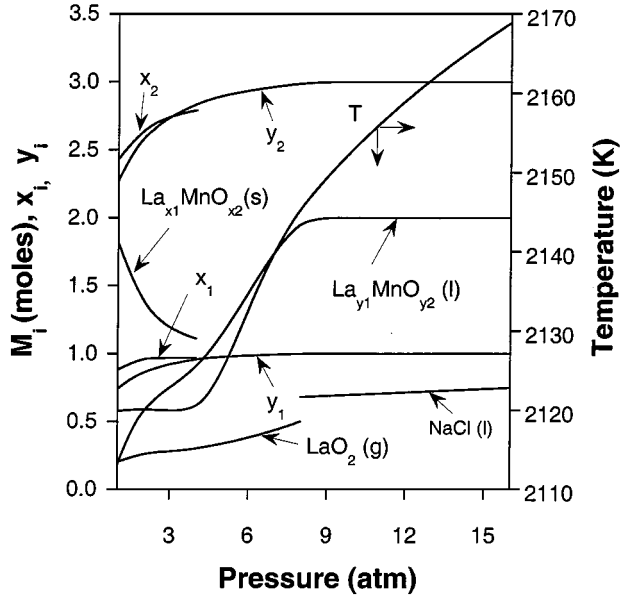

Figure 2 Dependence of the equilibrium temperature and composition of the products formed by the reaction mixture of $La_2O_3 + 2Mn + 0.75NaClO_4$.

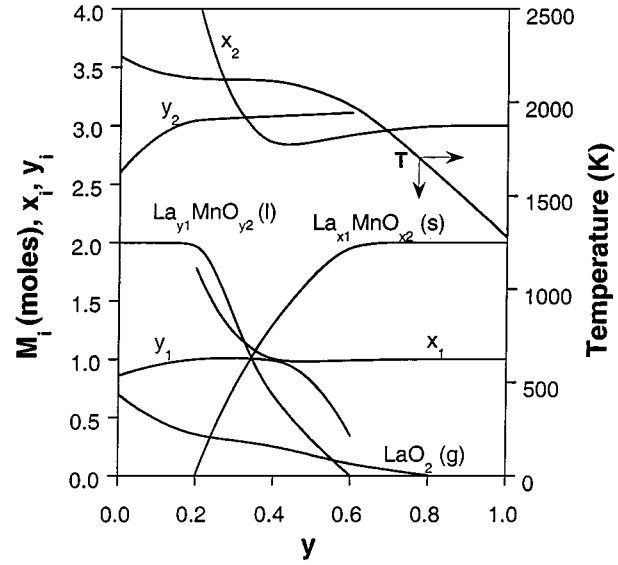

Figure 3 Dependence of the equilibrium temperature and composition of the products formed by the reaction mixture of $La_2O_3 + (2-y)Mn + yMnO_2 + O_2$.

TABLE I Calculated equilibrium temperatures of three products made by reactions (1–6) at 1 atm pressure

Compounds	Oxidant	Without dilution, $y = 0$	With dilution, $y = 0.8$
$LaMnO_3$	O_2	2246.0	1651.9
	$NaClO_4$	2120.0	1505.7
$La_{0.9}Sr_{0.1}MnO_3$	O_2	2242.7	1615.7
	$NaClO_4$	2120.2	1477.3
$La_{0.8}Sr_{0.2}MnO_3$	O_2	2177.4	1580.0
	$NaClO_4$	2113.7	1449.0

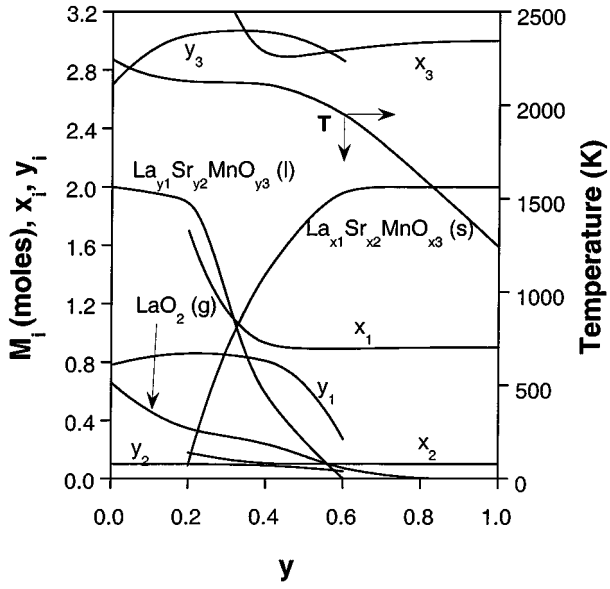

Figure 4 Dependence of equilibrium temperature and composition of the products formed by the reaction mixture of $0.9La_2O_3 + 0.2SrO_2 + (2 - y)Mn + yMnO_2 + O_2$.

oxidant decreases the combustion temperature due to the heat needed to evaporate the NaCl. The combustion temperature during the synthesis of $La_{0.9}Sr_{0.1}MnO_3$ exceeds that of the synthesis of $La_{0.8}Sr_{0.2}MnO_3$, since the second reaction requires decomposition of a larger amount of SrO_2.

The calculated combustion temperatures for both $LaMnO_3$ and $La_{1-x}Sr_xMnO_3$ ($x = 0.1$ and 0.2) are rather high using either $NaClO_4$ or oxygen as the oxidant, even at atmospheric pressure. Thus, it is feasible to generate a self-sustained combustion wave in these systems.

3. Experimental system and procedure

The following reactants were used to prepare the reactive mixtures: La_2O_3 (Alfa Aesar, average particle size ($\bar{\mu}$) smaller than 1 μm), SrO_2 (Aldrich, $\bar{\mu}$ smaller than 10 μm, ACS), Mn (Alfa Aesar, $\bar{\mu} = 9.85$ μm), and $NaClO_4$ (Alfa Aesar, $\bar{\mu} = 15$ μm). The green mixtures were prepared by 3 hours of dry mixing of the reactant powder in a ball mill (US Stoneware, Mahwah, NJ) with ZrO_2 balls. The combustion was conducted either in air for mixtures containing $NaClO_4$ or in an oxygen atmosphere (Trigas Co.). A special solid ignition mixture (chemical match) containing Al_2O_3, BaO_2 and Ti was used to initiate the SHS when using $NaClO_4$ as the oxidant. Some experiments were conducted using either loose powder or cylindrical pellets formed by pressing the powder mixture.

The phase composition and morphology of the samples were determined by X-ray diffraction (Siemens D5000), Scanning Electron Microscope and Electron Probe Microanalysis (JEOL JXA/8600) with a beam energy of 15 kV and a 30 nA current. Wavelength dispersive spectrometry was used for quantitative chemical analysis of the phases rather than EDAX due to its higher accuracy and precision. Synthetic and natural specimens were used to calibrate the X-ray. The data were processed using routines of the Geller Microanalytical Laboratory (Topsfield, Mass) and the ZAF matrix correction scheme of Armstrong. Thermal analysis was conducted with SEIKO TG/DTA 320 at a heating rate of 20 °C/min and a flow rate of 60 sccm of pure oxygen.

For inductive coupled plasma spectrometry, a 1.0000 gm ($\pm$0.0002) sample was dissolved in 12 N HCl on a hot plate. Following evaporation, the dry residue was re-dissolved in 1.5 N HNO_3 to yield a sample, which was analyzed. The ICP was calibrated by standard solutions, one solution per element. The electrical conductivity measurements were conducted by 4-terminal conductivity method.

4. Results and discussion

SHS of a mixture with the stoichiometric composition of $La_{0.9}Sr_{0.1}MnO_3$ yielded a multi-phase product. Following 2 hours of calcination at 1400 °C, the X-ray diffraction pattern of the powder shows the presence of some La_2O_3 peaks (Fig. 5). This agrees with reported results [21] that it is very difficult to prepare the stoichiometric $La_{0.9}Sr_{0.1}MnO_3$. However, a stoichiometric undoped $LaMnO_3$ product was readily prepared by calcination of SHS powder.

We studied mainly the synthesis of $La_{0.89}Sr_{0.1}MnO_3$, i.e., a product with a slight lanthanum deficiency which is recommended for use in solid oxide fuel cells. As dilution with MnO_2 decreases the combustion temperature, the initial experiments were conducted without it. The atmospheric SHS experiments with $NaClO_4$ were

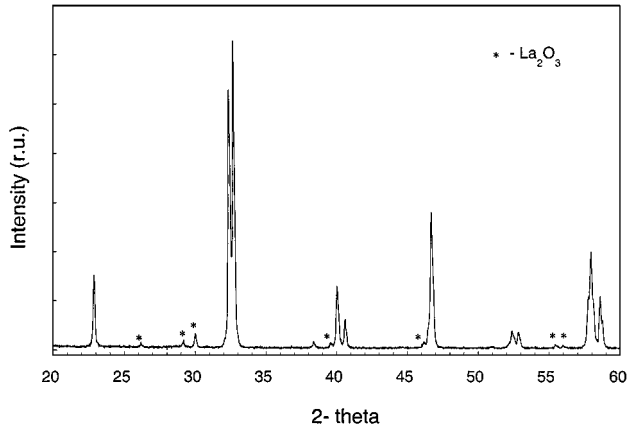

Figure 5 X-ray diffraction of $La_{0.9}Sr_{0.1}MnO_3$ made by the reaction mixture of $0.9La_2O_3 + 0.2SrO_2 + 2Mn + O_2$ after the calcination at 1400 °C for 2 hours.

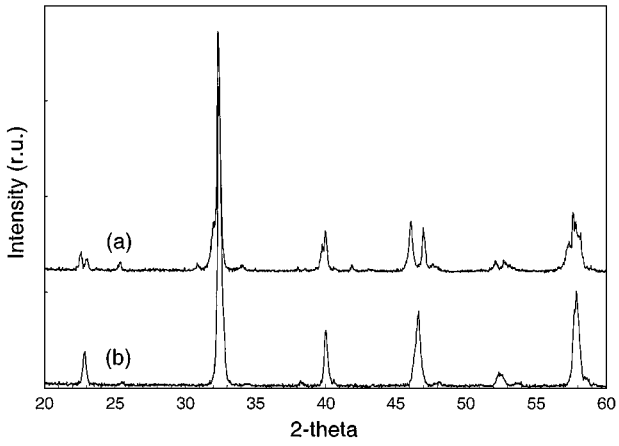

Figure 6 X-ray diffraction of SHS $La_{0.89}Sr_{0.1}MnO_3$ powder cooled in air (a) and cooled in furnace (b).

easier than those with gaseous oxygen, which had to be conducted at higher pressures.

Pellets with a diameter of 37.5 mm and 40 mm long were formed by pressing powder mixture containing $NaClO_4$ to about 40% of the theoretical density. The combustion was very intensive and the high temperature front propagated through the pellet in a few seconds. A large amount of white NaCl gases was released as the combustion wave passed through the pellet. The high temperature and gas evolution caused cracking of the product pellet and partial melting. X-ray diffraction of ground fine powder from the center of the pellet (Fig. 6a) does not show any La_2O_3 and Mn peaks, indicating complete conversion of these reactants. No NaCl was detected by either X-ray diffraction or EPM, indicating that all the NaCl evaporated during the combustion. TG/DTA [17] analyses indicate that $NaClO_4$ decomposes at 480 °C and NaCl evaporates at 1413 °C. The combustion temperature of about 1850 °C of this reaction mixture (Fig. 2) highly exceeds the evaporation temperature of NaCl. Comparison of the X-ray diffraction pattern with that of a standard sample indicates that the main product is the desired phase with some intermediate impurities. We conjecture that the presence of intermediates was due to the short period the product was at the high temperature (less than one minute).

To check the impact of the sample cooling, a piece of the combusted LSM sample was placed in a pre-heated furnace (1500 °C) and the power turned off. The furnace temperature remained above 750 °C for about 90 minutes, below which the reaction rate was negligible. The X-ray diffraction pattern of the sample (Fig. 6b) shows that heating increased the LSM purity. This suggests that combustion of a large diameter batch, the cooling rate of which is similar to that of the furnace, will generate a high purity product and will not require post treatment.

SHS of LSM in O_2 led to a higher purity product than from a reactant mixture containing $NaClO_4$ because of the higher combustion temperature, as predicted by TFA. The combusted pellet did not crack and kept its shape since no gaseous compounds formed during the combustion.

When SHS of a loose powder mixture was conducted in a flowing oxygen stream, the sample remained at a high temperature for a longer period than the sample containing $NaClO_4$ and combusted in air. The X-ray diffraction pattern showed that the longer the period the combusted sample stayed at the high temperature the higher the homogeneity of the product.

Increasing the pellet density decreased the heat loss from the combusted sample, increased the contact among reactant particles, and favored the formation of homogeneous products. However, diffusion of O_2 into the center of a pellet with a high density is critical for conducting SHS. High pressure enhances the oxygen diffusion into the center of the pellet. X-ray diffraction of the central part of a 40 mm diameter pellet showed that an increase in the pressure increased the degree of crystallization and product purity.

The temperature at the pellet center is generally higher than that at the surface due to the heat loss (radiation and convection) from the surface. In general, a temperature gradient exists across the sample and the product homogeneity in the center is higher than at the surface. SHS in an O_2 environment generated three different zones in the pellet. Fig. 7a–c show BEI of these three regions. A partial melting in the pellet center caused homogenization (Fig. 7a). No partial melting occurred in the region next to the pellet surface and some unreacted La_2O_3 was present (Fig. 7c). The combustion temperature in the transition zone (Fig. 7b) was higher than in sintering zone, and the reaction proceeded further than in the sintering zone, some impurity of $(La_{1-x}Sr_x)_2MnO_4$ was present in an intermediate zone. The relative size of the three zones depended on the pellet density, oxygen pressure and sample parameters.

A TG/DTA analysis of metal manganese in a pure oxygen environment (Fig. 8) showed that a rapid oxidation of the manganese started at about 550 °C. This ignited the metal and generated a large exothermic peak. If heat from the combustion front does not increase the temperature of the adjacent layer to the ignition temperature of Mn, extinction will occur even when the O_2 supply is sufficient. The propagation of the combustion wave is strongly dependent on the metal oxidation. In general, at low oxidation temperatures the combustion front movement tends to be more regular and steady.

The sequence of chemical and phase transformation during the SHS was studied by quenching the reaction front in a conical combustion-wave arresting setup [15], using a reactant mixture containing $NaClO_4$. Our previous TG/DTA analyses [17] indicated that $NaClO_4$ decomposes at 480°C and releases a large amount of the heat and that the decomposition of SrO_2 starts at 431°C and again at 800°C, forming SrO. Layer by layer X-ray diffraction and electron probe microanalysis suggested the following sequence of reactions occur. In the layer ahead of the combustion front, $NaClO_4$ and SrO_2 decompose by the reactions:

$$NaClO_4 \rightarrow 2O_2 + NaCl\uparrow \quad (7)$$

$$SrO_2 \rightarrow SrO_x + 1/2O_2 \quad (8)$$

The active O_2 released from these decompositions and heat conduction from the high temperature zone cause rapid oxidation of the metallic Mn. This oxidation

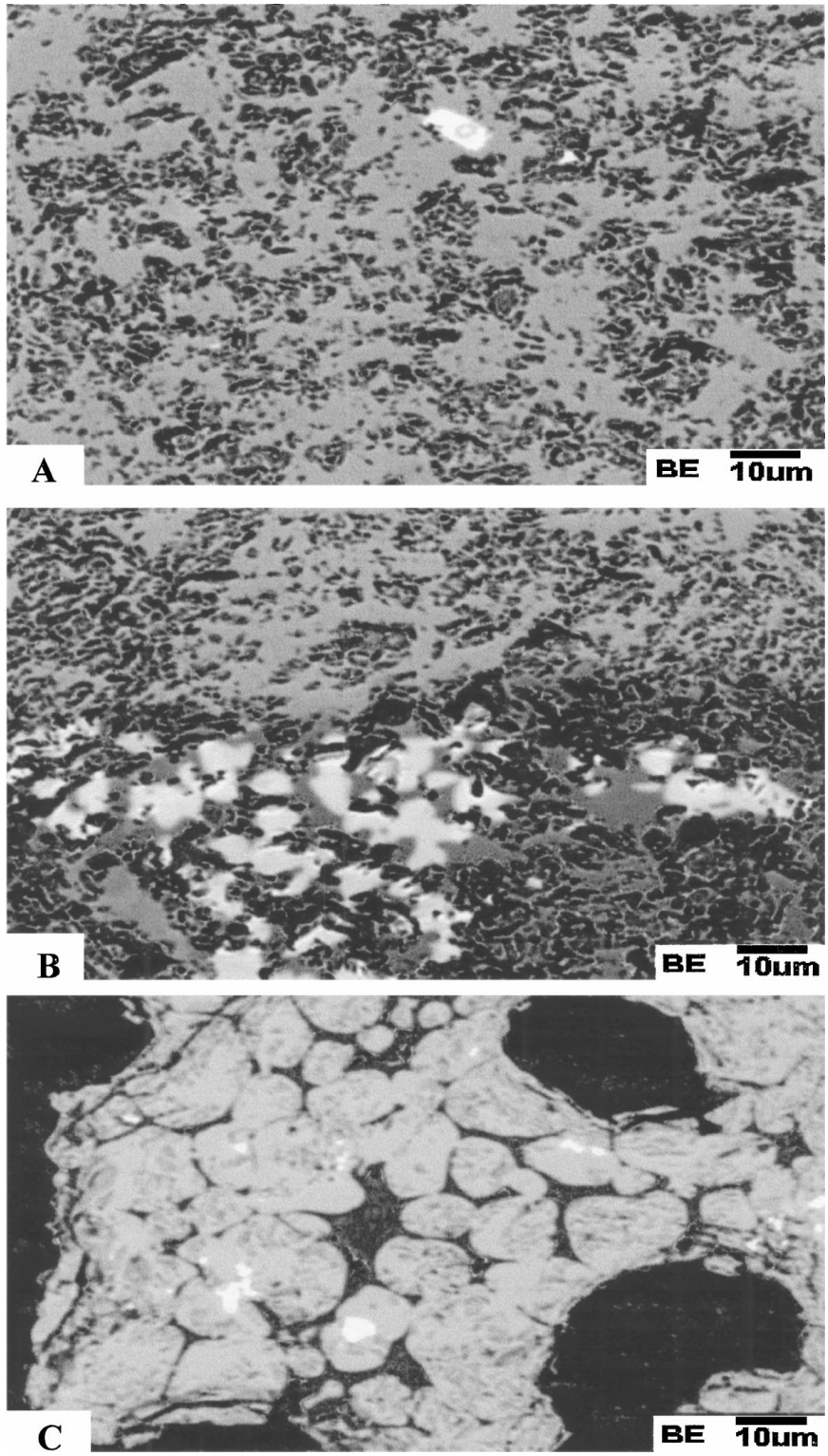

Figure 7 Back scattered electron images of product of the reaction $0.89La_2O_3 + 0.2SrO_2 + 2Mn + O_2$ with diameter 40 mm (a) sample center (note that white area is unreacted La_2O_3 due to non homogeneous mixture), (b) about 15 mm from pellet center and (c) next to pellet surface.

releases a large amount of heat (Fig. 8) inducing a combustion front in the adjacent layer. The analyses of the combustion front zone by X-ray diffraction and EPMA indicate that an Mn_2O_3 intermediate is formed by the oxidation of Mn:

$$2Mn + 1.5O_2 \rightarrow Mn_2O_3 \qquad (9)$$

At the high temperature zone, La_2O_3 and Mn_2O_3 participate in the reaction:

$$(1 - x)La_2O_3 + Mn_2O_3 \xrightarrow{O_2} 2La_{1-x}MnO_3 \qquad (10)$$

Sr is incorporated into the perovskite by the reaction:

$$La_{1-x}MnO_3 + xSrO \rightarrow La_{1-x}Sr_xMnO_3 \qquad (11)$$

The presence of $(La_{1-x}Sr_x)_2MnO_4$ suggests that one of the following reactions or both may have occurred,

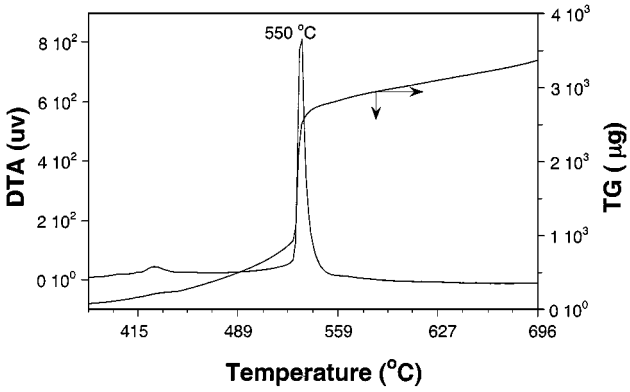

Figure 8 TG/DTA of manganese metal with a heating rate of 20 °C/min and oxygen flow rate of 60 ml/min.

$$La_2O_3 + SrO + Mn_2O_3 \rightarrow (La_{1-x}Sr_x)_2MnO_4 \quad (12)$$

$$La_{1-x}Sr_xMnO_3 + SrO + La_2O_3 \rightarrow (La_{1-x}Sr_x)_2MnO_4 \quad (13)$$

$(La_{1-x}Sr_x)_2MnO_4$ then react with Mn_2O_3

$$(La_{1-x}Sr_x)_2MnO_4 + Mn_2O_3 \rightarrow La_{1-x}Sr_xMnO_3 \quad (14)$$

The final desired composition of $La_{0.89}Sr_{0.1}MnO_3$ and its homogenization occur in the final combustion stage.

The LSM powder used in solid oxide fuel cell must satisfy certain specifications, such as microstructure, purity, sinterability and electrical conductivity. LSM produced by SHS of a 40 mm diameter and 40 mm long sample of a slightly pressed powder mixture in an O_2 pressure of 4 psi was ground to a powder to an average particle size of 10–15 μm, and then pressed to form a cylindrical pellet of 37.5 mm diameter. This pellet was heated to 1400 °C at a heating rate of 5 °C/min and calcined at this temperature for 3 hours and then cooled at the same rate. About 25-gram of the crushed parts of the calcined pellet in isopropanol were ground for 35 minutes with two WC grinding balls in a 300 ml volume WC vial placed in a Spex-8000 grinding machine. The product (Fig. 9) had a uniform particle size

TABLE II ICP analysis of the $La_{0.89}Sr_{0.1}MnO_3$ product

Element	ICP results, wt%	Absolute Std. Dev wt%	Relative % Std. Dev.	Cations per Mn
La	58.04	±0.19	±0.3	0.89 ± 0.006
Sr	4.19	±0.01	±0.3	0.1 ± 0.0006
Mn	25.86	±0.08	±0.3	1.00

TABLE III Impurity concentrations in the $La_{0.89}Sr_{0.1}MnO_3$ product

Element	ICP results (ppm)	Absolute Std. Dev. (ppm)	Relative Std. Dev. %
Si	62	±0.7	±1.1
Al	51	±1.9	±3.4
Cu	31	±0.4	±1.4
Ca	55	±0.4	±0.4
Mg	19	±0.2	±1.2
Fe	55	±0.3	±0.6
Total	273	—	—

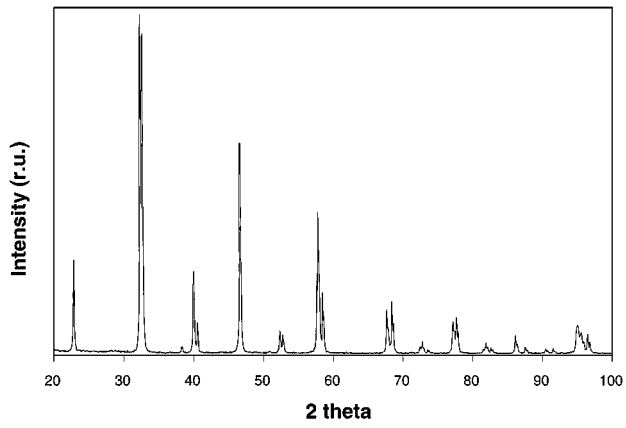

Figure 10 X-ray diffraction of powder made by SHS of the mixture of $0.89La_2O_3 + 0.2SrO_2 + 2Mn + O_2$.

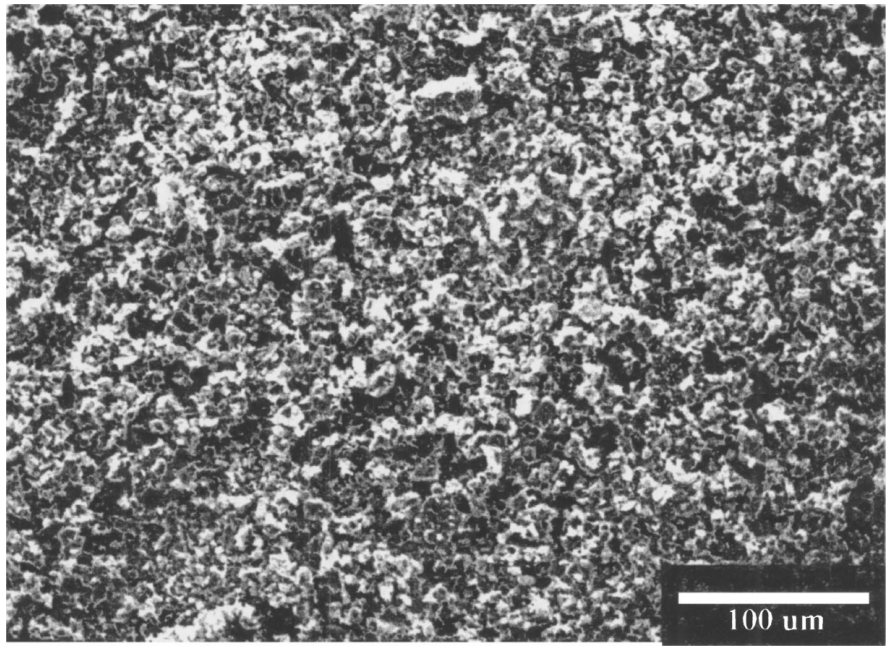

Figure 9 SEM of powder made by SHS of the mixture of $0.89La_2O_3 + 0.2SrO_2 + 2Mn + O_2$.

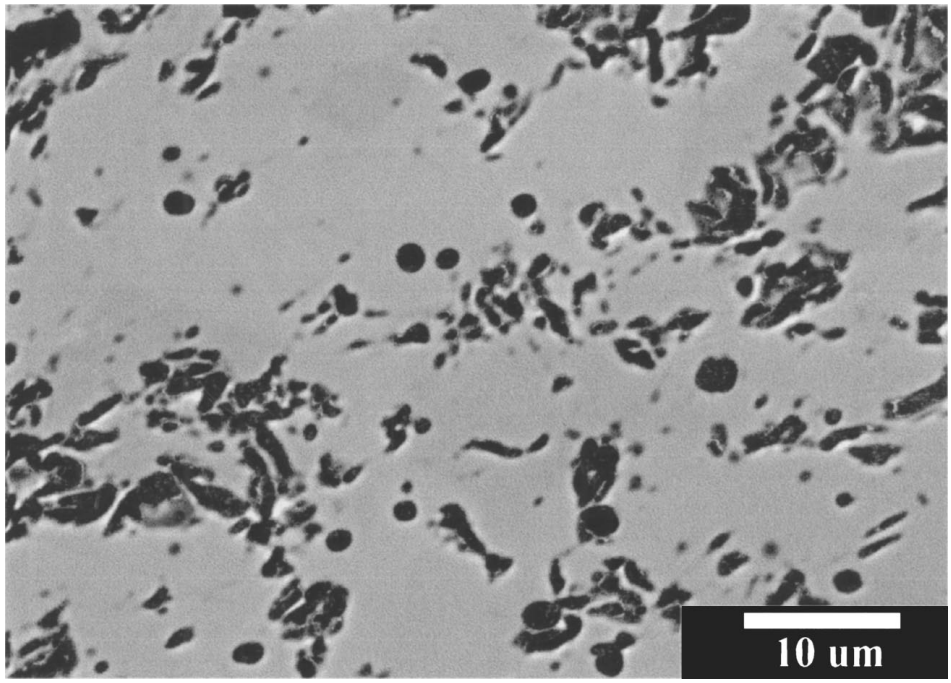

Figure 11 EPMA powder made by SHS of the mixture of $0.89La_2O_3 + 0.2SrO_2 + 2Mn + O_2$.

distribution with an average size of about 10 μm, determined by Mastersizer (Malvern Instruments Inc., MA). X-ray diffraction (Fig. 10) and Electron probe microanalysis showed that this powder was a single phase. The corresponding BEI with a uniform average Z contrast is shown in Fig. 11. Wavelength dispersive spectrometry analysis indicated that the product composition was $La_{0.89}Sr_{0.1}MnO_3$.

The stoichiometry of the La, Sr, Mn and O of SHS product $La_{0.89}Sr_{0.1}MnO_3$ was determined by inductively coupled plasma spectrometry. The stoichiometry of the LSM powder is reported in Table II and the corresponding impurity concentration in Table III. The product stoichiometry of $0.89 : 0.1 : 1$ is same as of the reactant mixture. The total impurity concentrations of 273 ppm is much smaller than the specified maximum of 1000 ppm. The SHS does not involve many intermediate processing steps, except grinding and calcination. Thus it minimizes the possibility of inserting impuritis into the product. Also, volatile elements are removed from the product during SHS due to the very high combustion temperature. The electrical conductivity of the product of 180 $S{\cdot}cm^{-1}$ at 1000 °C in air matches that of the available commercial product.

5. Conclusions

Thermodynamic analyses have predicted and experiments confirmed that a high quality $La_{1-x}Sr_xMnO_3$ can be prepared via SHS. The predicted combustion and melting temperatures of the product were in good agreement. The intermediate products for both green mixtures $La_2O_3 + SrO_2 + Mn + NaClO_4$, $La_2O_3 + SrO_2 + Mn$, in oxygen include $LaMnO_3$, $(La_{1-x}Sr_x)_2MnO_4$ and Mn_2O_3. The high combustion temperature caused partial melting, which increased the product homogeneity at low oxygen pressure. A homogeneous product was obtained by calcination of the SHS product at 1400 °C for 3 hours. A product powder with an average particle size of 10 μm and a narrow particle size distribution was obtained by grinding the SHS product for 35 minutes. The total impurity concentrations of 273 ppm is much smaller than that of the specified maximum of 1000 ppm. The electrical conductivity of 180 $S{\cdot}cm^{-1}$ at 1000 °C in air matches that of commercial product made by other processes.

Acknowledgements

This work was supported by the Texas Center for Superconductivity, the Materials Research Science and Engineering Center program of the National Science Foundation under Award Number DMR-9632667 and by a grant from the Defense Advanced Research Project Agency.

References

1. S. C. SINGHAL, in 17th Risø International Symposium on Materials Science, High Temperature Electrochemistry, Roskilde, Denmark, September 1996. Reprinted from Ceramics and Metals.
2. M. P. PECHINI, U.S. Patent # 3,330,697 (1967).
3. H. U. ANDERSON, C. C. CHEN, J. C. WANG and M. J. PENNELL, in "Ceramic Powder Science III" edited by G. L. Messing, S. I. Hirano and H. Hausner (American Ceramic Society, Westerville, OH, 1990) p. 749.
4. L. W. TAI and P. A. LESSING, *J. Mater. Res.* **7** (1992) 502.
5. C. MARCILLY, P. COURTY and B. DELMON, *J. Amer. Ceram. Soc.* **53** (1970) 56.
6. P. SUJATHA DEVI, *J. Mater. Chem.* **3** (1993) 373.
7. D. W. JOHNSON, JR., P. K.GALLAGHER, F. SCHREY and W. W. RHODES, *Amer. Ceram. Soc. Bull.* **55** (1976) 520.
8. N. CHRISTIANSEN and P. GORDES, in Proceedings of the Second International Symposium on Solid Oxide Fuel Cell, Athens, Greece, July 2–5, 1991, edited by F. Grosz, P. Zegers and S. C. Singhal (Commission of European Communities, Luxembourg, 1991) p. 495.
9. I. A. AKSAY, G. D. MAUPIN, C. B. MARTIN, R. P. KUROSKY and G. C. STANGLE, U.S. Patent no. 5061682, Oct. 29 (1991).
10. E. SUSKAKIS, S. BILGER and A. NAOUMINDIS, in Proceedings of the Second International Symposium on Solid Oxide Fuel Cell, Athens, Greece, July 2–5, 1991, edited by F. Grosz, P. Zegers and S. C. Singhal (Commission of European Communities, Luxembourg, 1991) p. 787.

11. H. TAGUCHI, D. MATSUDA and M. NAGAO, *J. Amer. Ceram. Soc.* **75** (1992) 201.
12. L. A. CHICK, L. R. PEDERSON, G. D. MAUPIN, J. L. BATES, L. E. THOMAS and G. J. EXARHOS, *Mater. Lett.* **10** (1990) 6.
13. A. G. MERZHANOV, in "Combustion and Plasma Synthesis of High-Temperature Materials" edited by Z. A. Munir and J. B. Holt (VCH Publ., New York, 1990) p. 1.
14. P. B. AVAKYAN, M. D. NERSESYAN and A. G. MERZHANOV, *Amer. Ceram. Soc. Bull.* **75**(2) (1996) 50.
15. Q. MING, M. D. NERSESYAN, R. KENT, J. T. RICHARDSON and D. LUSS, *Combust. Sci. and Tech.* **128** (1997) 279.
16. Q. MING, J. HUNG, Y. L. YANG, M. NERSESYAN, A. J. JACOBSON, J. T. RICHARDSON and DAN LUSS, *ibid.* **138** (1998) 279.
17. Q. MING, M. D. NERSESYAN, S. LIN, J. T. RICHARDSON and D. LUSS, *Int. J. SHS* **7**(4) (1998) 447.
18. Q. MING, Y. L. YANG, A. WANGER, J. RITCHIE, M. D. NERSESYAN, A. J. JACOBSON, J. T. RICHARDSON and D. LUSS, *Solid State Ionics* **122** (1999) 113.
19. A. A. SHIRYAEV, *Int. J. SHS* **4**(4) (1995) 351.
20. A. A. SHIRYAEV, M. D. NERSESYAN, Q. MING and D. LUSS, *J. Mater. Syn. and Proc* **7**(2) (1999) 85.
21. N. Q. MINH and T. TAKAHASHI, "Science and Technology of Ceramic Fuel Cell" (Elsevier, New York, 1995) p. 123

Received 10 March
and accepted 16 August 1999